PROCEEDINGS OF SPIE

SPIEDigitalLibrary.org/conference-proceedings-of-spie

Detecting and segmenting overlapping red blood cells in microscopic images of thin blood smears

Golnaz Moallem, Hamed Sari-Sarraf, Mahdieh Poostchi, Richard J. Maude, Kamolrat Silamut, et al.

Golnaz Moallem, Hamed Sari-Sarraf, Mahdieh Poostchi, Richard J. Maude, Kamolrat Silamut, Md Amir Hossain, Sameer Antani, Stefan Jaeger, George Thoma, "Detecting and segmenting overlapping red blood cells in microscopic images of thin blood smears," Proc. SPIE 10581, Medical Imaging 2018: Digital Pathology, 105811F (6 March 2018); doi: 10.1117/12.2293762

SPIE.

Event: SPIE Medical Imaging, 2018, Houston, Texas, United States

Detecting and Segmenting Overlapping Red Blood Cells in Microscopic Images of Thin Blood Smears

Golnaz Moallem[a], Hamed Sari-Sarraf[a], Mahdieh Poostchi[b], Richard J. Maude[c d], Kamolrat Silamut[c], Md Amir Hossain[e], Sameer Antani[b], Stefan Jaeger[b], George Thoma[b]
[a] Electrical and Computer Engineering Department, Texas Tech University, Lubbock, USA; [b] Lister Hill National Center for Biomedical Communications, U.S. National Library of Medicine, Bethesda, USA; [c] Mahidol-Oxford Tropical Medicine Research Unit, Mahidol University, Bangkok, Thailand; [d] Nuffield Department of Clinical Medicine, University of Oxford, Oxford, United Kingdom; [e] Chittagong Medical College & Hospital, Chittagong, Bangladesh

ABSTRACT

Automated image analysis of slides of thin blood smears can assist with early diagnosis of many diseases. Automated detection and segmentation of red blood cells (RBCs) are prerequisites for any subsequent quantitative high-throughput screening analysis since the manual characterization of the cells is a time-consuming and error-prone task. Overlapping cell regions introduce considerable challenges to detection and segmentation techniques. We propose a novel algorithm that can successfully detect and segment overlapping cells in microscopic images of stained thin blood smears. The algorithm consists of three steps. In the first step, the input image is binarized to obtain the binary mask of the image. The second step accomplishes a reliable cell center localization that utilizes adaptive meanshift clustering. We employ a novel technique to choose an appropriate bandwidth for the meanshift algorithm. In the third step, the cell segmentation purpose is fulfilled by estimating the boundary of each cell through employing a Gradient Vector Flow (GVF) driven snake algorithm. We compare the experimental results of our methodology with the state-of-the-art and evaluate the performance of the cell segmentation results with those produced manually. The method is systematically tested on a dataset acquired at the Chittagong Medical College Hospital in Bangladesh. The overall evaluation of the proposed cell segmentation method based on a one-to-one cell matching on the aforementioned dataset resulted in 98% precision, 93% recall, and 95% F1-score index.

Keywords: cell detection, cell segmentation, meanshift clustering, snake active contour, red blood cell segmentation

1. INTRODUCTION

Enumeration and segmentation of cells in microscopic images provides useful information for many different applications. For example, the slides of stained peripheral thin blood smears are analyzed to assist with diagnosis of blood disorders. In the slides of thin blood smears, three types of cells appear: white blood cells (leukocytes), red blood cells (erythrocytes), and platelets (thrombocytes). Red blood cells (RBCs) are disk-shaped, nucleus-less cells in the blood that carry oxygen throughout the human body. The average disk diameter of a typical human RBC is approximately 6-8 μm. Any irregularity regarding the count of RBCs may be a sign of conditions such as hemolytic anemia, polycythemia

Medical Imaging 2018: Digital Pathology, edited by John E. Tomaszewski, Metin N. Gurcan,
Proc. of SPIE Vol. 10581, 105811F · © 2018 SPIE · CCC code:
1605-7422/18/$18 · doi: 10.1117/12.2293762

and leukemia[1]. Moreover, abnormalities relating to shape, size, texture and/or color of the cells observed in a microscopic image can lead to diagnosis of several pathological conditions such as sickle cell disease, thalassemia and malaria infection [1].

Manually detecting and segmenting red blood cells in microscopic images of thin blood smears by visual inspection is a tedious, time consuming and error-prone task. On the other hand, automated algorithms for cell detection and segmentation have proven useful in supplementing or even substituting the manual process [2, 3]. However, the presence of overlapping cells is known to adversely affect the automatic detection and segmentation process.

It is therefore not surprising that the segmentation of single and overlapping RBCs has been and continues to be extensively studied. Algorithms based on Otsu thresholding [4-12], edge detection [13] and quaternion Fourier transform [14] have been employed, yet they have shown limitations with regard to high color and textural variations. Active contour models [15, 16], PCNN-based RBC segmentation [17, 18], K-means clustering [19, 20] and Poisson distribution thresholding [21] have been found to fall short of handling overlapping RBCs regions. Watershed has been widely used for RBCs segmentation [5, 22, 23], nonetheless it has shown a tendency towards oversegmentation. To solve this problem, marker-controlled watershed algorithms have been introduced [24-26], although marker-controlled watershed methods can address the oversegmentation problem successfully only if the extracted markers represent the actual objects. Hough transform [27-30], ellipse fitting [31], granulometry [8, 32] and rule-based approaches [33, 34] have been employed effectively in segmentation of overlapping regions; however, since these methods make restrictive shape assumptions, cell shape information may be distorted. The objective of this paper is to develop a new algorithm that can improve detection and segmentation of overlapping RBCs in microscopic images of thin blood smears.

2. METHODOLOGY

In this work, we present a novel methodology that successfully performs detection and segmentation of RBCs, including overlapping cells. The three main steps of this algorithm are preprocessing, cell detection by adaptive meanshift clustering, and cell segmentation using GVF-driven snake active contours (Gradient Vector Flow). The output of the preprocessing step is the binary mask of the input image where RBCs appear as white blobs. In the cell detection step, an adaptive meanshift algorithm localizes the geometric centers of the cells using the obtained binary mask. An appropriate bandwidth for the mean shift algorithm is chosen automatically by our proposed method. Finally, in the cell segmentation step, the presented cells in the binary mask are segmented utilizing a GVF-driven deformable snake method. Figure 1 demonstrates the flowchart of the overall algorithm for detection and segmentation of overlapping RBCs. Each step is explained in the following subsections and the result of each step is demonstrated on a sample image from the dataset we used in our experiments.

Figure 1. The flowchart of the overall algorithm

2.1 Preprocessing

Our proposed preprocessing step outputs the binary mask of the input image in order for it to be used in the subsequent meanshift clustering step. The preprocessing step involves five stages. In the first stage, the region of interest (ROI), i.e., the non-black region in the image that is visible through the microscope, is extracted from the image and subsampled by the factor of 1/4 for the benefit of computational speed. In the second stage, principal component analysis (PCA) is used to reduce the dimensionality of the RGB space down to one [35]. PCA is applied to the raw matrix of pixel values in which each row corresponds to an individual pixel's RGB intensity values. Applying PCA in this manner results in a 3x3 coefficient matrix in which each column consists of coefficients for one principal component in descending order of component variance. PCA coefficients corresponding to the largest component variance are used to obtain the grayscale intensity value for each pixel. Therefore, at this point, the grayscale version of the image is obtained. In the third stage, the subsampled grayscale image is binarized by replacing all the intensity values above a globally determined threshold with zeros and setting all the other values to ones. The global threshold for binarization is calculated using Otsu's method [36]. This method assumes that the image contains two classes of pixels following a bimodal histogram and calculates the optimum threshold separating the two classes where the inter-class variance is maximal. As the representative example in Figure 2 shows, Otsu's method is an appropriate choice of thresholding for our application. The purpose of binarization is to obtain the binary mask of the subsampled image, in which the cells appear as connected and preferably isolated blobs. Through the fourth stage, the binary mask is refined. In many of our images, there are cells that have distorted translucent regions within them, known as pallor zones [37]. The pallor zones manifest themselves as holes within the blobs after binarization and are removed from consideration by morphological filling. In the last stage, a size filter is used to remove impertinent blobs from the mask image that may correspond to contamination from the staining and/or imaging process or even blood components such as platelets. Since the average diameter of a platelet is around 2-4 μm, i.e., less than half of the diameter of an average RBC, the size of an average platelet is approximately one fourth of that of an average RBC. Therefore, the size threshold in this experiment is set around one fourth of the average area of a single RBC. The average area of a RBC is estimated manually from the images in the dataset that were used in our experiments. Figure 3 shows the results of all the stages of the preprocessing step.

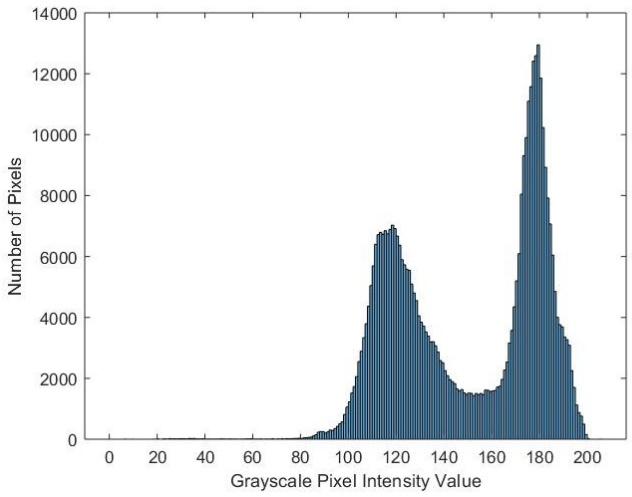

Figure 2. Histogram of the grayscale version of the sample image shown in Fig. 3a

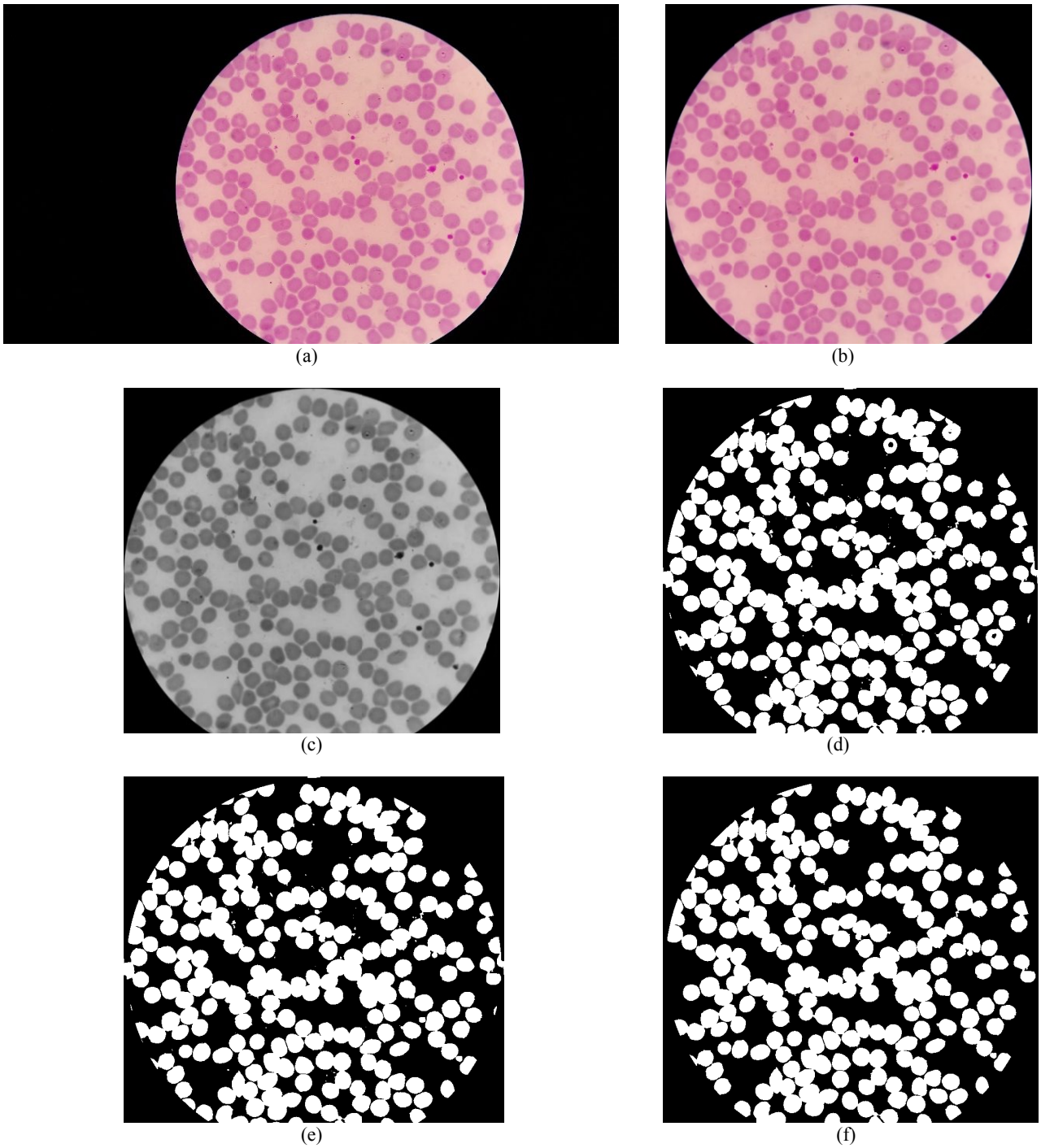

Figure 3. Preprocessing: (a) sample image, (b) ROI extraction & subsampling, (c) PCA grayscale conversion, (d) binarization, (e) binarization refinement by morphological filling, and (f) size filtering.

2.2 Cell Detection

In the second step of the algorithm, an adaptive meanshift algorithm is used to localize the center of the RBCs [38]. In the context of our application, the meanshift algorithm serves as a clustering tool to obtain the centers and the corresponding pixel labels of the cells present in the binary mask of the input image. The meanshift algorithm is based on kernel density estimation (KDE), where a kernel with a certain bandwidth value is translated to each data point in the dataset and all such kernels are summed to form the KDE surface. Different kernel bandwidth values will result in different KDE surfaces that lead to different meanshift results. Therefore, the KDE surface and, consequently, the meanshift algorithm depend on the used kernel bandwidth. To perform meanshift algorithm, the kernel bandwidth and the input data points must be provided. The binary mask obtained in the previous step provides the data points that are used to construct the input to the meanshift algorithm. To form the input data points, first, the distance map of the binary mask is calculated. The distance transform of each pixel in the binary mask is its distance to the nearest background pixel. All white pixels in the binary mask have distance values greater than zero. A list of these pixels is formed to establish a matrix called the weighted input matrix. In the weighted input matrix, each pixel in the list is repeated as many times as its distance value calculated from the topographic surface of the binary mask. This weighted input matrix is used as the input data points to the meanshift algorithm. The reason behind this phase of the algorithm is to create a denser data cloud for the meanshift algorithm. In other words, this step generates a more accurate KDE surface for the meanshift algorithm. For microscopy images of RBCs with an average cell radius of R, our experiments indicate that if the meanshift algorithm is implemented iteratively with bandwidth values equal to λR, with λ in the range of [0.5, 0.9], and a step size of $k = 0.1$, the estimates, i.e., the computed number of clusters, exhibit an optimal bias-variance relationship. With this in mind, we introduce a novel algorithm to select the proper bandwidth for the meanshift procedure. In this method, for each image, the meanshift algorithm is performed on the obtained weighted data matrix with the following values of bandwidths: 0.5R, 0.6R, 0.7R, 0.8R and 0.9R. The number of clusters generated by the meanshift algorithm for each bandwidth is stored. This process is repeated for radii equal to R-2, R-1, R, R+1 and R+2 and the results are tabulated as a matrix called the bandwidth selection matrix. Afterwards, we find the most frequent value (MVF) in the bandwidth selection matrix. At last, looking into the row corresponding to R, we find the bandwidth that produces the MVF. This is the bandwidth that is chosen for the meanshift algorithm for this particular image. Then, the meanshift algorithm is executed, employing the chosen bandwidth to generate the center locations of the cells and the label for each data point.

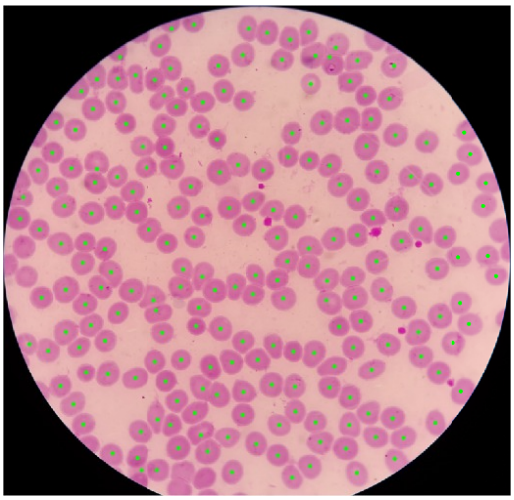

Figure 4. Generated cell centers marked green on the ROI of the sample image

In Figure 4, centers of the cells as generated by the meanshift algorithm are plotted on the ROI of the sample image. Since the data points are labeled after the meanshift procedure, we are able to find the pixels located on the boundary of each cell. These pixels represent the partial boundary of the corresponding cell. To obtain the partial boundary of the k^{th} cell, the mutual pixels between the edge map of the binary image and the pixels within the k^{th} cell are determined. In other words, the data points within the k^{th} cluster that belong to the edge map of the binary mask represent the partial boundary of the corresponding cell. Figure 5 demonstrates the derived partial boundaries marked on all the cells in the ROI of the sample image. For more detailed explanation of this step, please refer to [39].

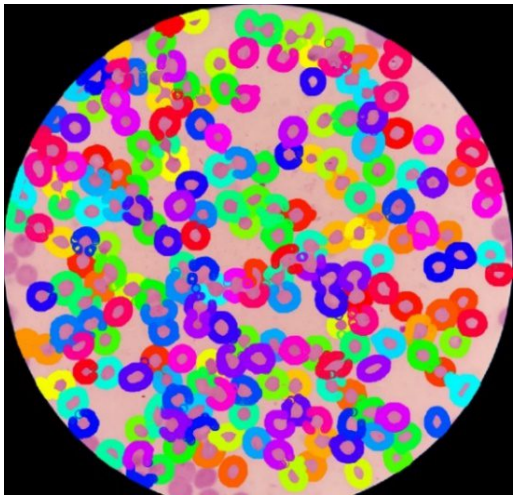

Figure 5. Extracted partial boundaries marked on the cells in the ROI of the sample image

2.3 Cell Segmentation

The last step of the algorithm estimates full boundaries of the RBCs utilizing a GVF-driven Snake algorithm [40]. GVF-driven snakes can be initialized both inside and outside of the object and can successfully handle partial boundaries. These two properties make this method a suitable choice for our application since there are cases of partial boundaries derived in the previous step. Having the partial boundary of individual cells accumulated in the previous step, GVF-driven snake is performed individually on the derived partial contour of each cell from the binary mask. For each cell, a mask is generated where only the partial boundary pixels of the corresponding cell are white. In this mask, the active contour is initialized as a circular curve located at the center of the cell with a sufficiently small radius to fit inside the cell (e.g. 3 pixels). As mentioned, all the cell center locations are calculated through the meanshift procedure. The evolution of the GVF-driven snake is terminated when it reaches the partial boundary pixels. The resultant curve is the estimated boundary of the corresponding cell. The algorithm repeats this process for all the cells present in the image. Figure 6 illustrates the acquired segmentation boundaries of all the cells marked on the sample image. For more comprehensive elaboration of this step, please refer to [39].

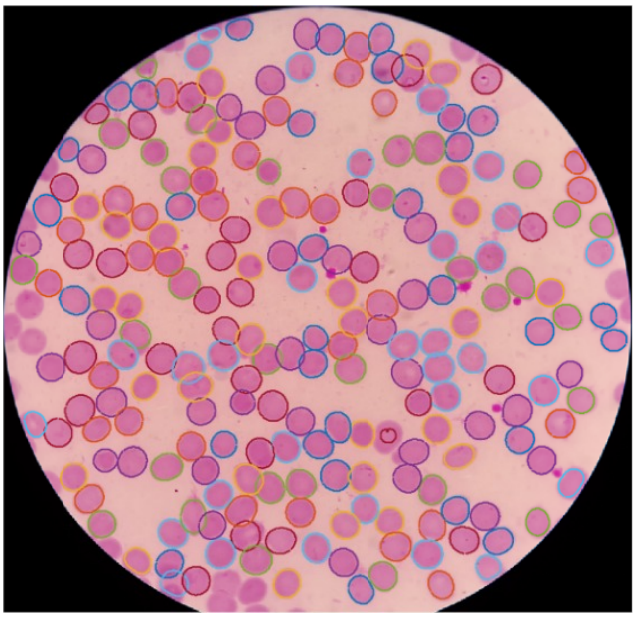

Figure 6. Obtained segmentation boundaries marked on the ROI of the sample image

3. MATERIAL & DATA

For this experiment, we use archived thin blood smear images acquired from Chittagong Medical College & Hospital in Bangladesh from 202 patients with and without P. falciparum infection [41, 42]. This set contains more than 1200 images comprising over 213,000 RBCs in total, with many overlapping cell regions. The average number of RBCs in a single image is 191.9. All images are in RGB color space obtained using a smartphone mounted on a regular light microscope. All the RBCs in the entire dataset are annotated manually by an experienced slide reader using the Firefly annotation tool (firefly.cs.missouri.edu).

4. RESULTS

The results illustrated in Figure 7 demonstrate the strength of the proposed algorithm in detecting touching and overlapping RBCs. The combination of partial boundary extraction and GVF-driven snake algorithm delivers an accurate cell segmentation performance. The derived boundaries are an accurate estimation of the cell morphology.

We compared the results of our algorithm with the results of three other state-of-the-art methods [7], [43] and [44]. To quantitatively compare, we performed a one-to-one matching between manually annotated cells and segmented cells. In this assessment, a segmented cell is considered a TP (True Positive) if there is a cell annotation within the segmented region of the corresponding cell, otherwise it is considered to be a FP (False Positive). Any undetected cell is considered a FN (False Negative). The overall evaluation of the algorithm on the aforementioned dataset based on the one-to-one cell matching results in 98% precision, 93% recall and 95% F1-score index that outperforms the Otsu thresholding method introduced in [7] with 84% precision, 81% recall, and 82% F1-score index, and also the marker-controlled watershed algorithm proposed in [43] with 93% precision, 95% recall, and 94% F1 index. Moreover, the

results of our algorithm are comparable with the ones obtained by the edge profile active contour and colored graph-based coupling algorithm presented in [44] with 94% precision, 96% recall, and 95% F-score. These results are tabulated in Table 1.

Table 1. The overall segmentation results compared with the ground truth annotations

Method	Precision	Recall	F1-score
Otsu Thresholding [7]	84%	81%	82%
Marker-controlled Watershed [43]	93%	95%	94%
[44]	94%	96%	95%
Proposed method	**98%**	93%	**95%**

To evaluate the performance of the bandwidth selection method, the algorithm was also tested on the entire dataset, with the meanshift algorithm employing the constant bandwidth value of 0.6R. The quantitative metrics were again calculated based on one-to-one matching. The results in Table 2 indicate that our proposed method for bandwidth selection strongly improves the overall results since it significantly decreases the number of falsely detected RBCs.

Table 2. Quantitative comparison of our bandwidth selection method with static bandwidth meanshift.

Method	Precision	Recall	F1-score
Constant bandwidth value of 0.6R for meanshift algorithm	**92%**	94%	**93%**
Our proposed bandwidth selection method for meanshift algorithm	**98%**	93%	**95%**

5. CONCLUSION

In this work, we introduced an algorithm that successfully performs detection and segmentation of RBCs. The proposed algorithm for cell detection employs an adaptive meanshift clustering technique that is capable of detecting multiple overlapping cells. It provides the number of cells present in an image, which can then be used for clinical purposes. We propose a novel method to select the bandwidth for the meanshift algorithm. Our method for cell segmentation utilizes GVF-driven snakes to segment cells accurately and obtain their boundaries. The results on our dataset demonstrate that the method yields superior or comparable segmentation performance compared to the results of other state-of-the-art methods.

ACKNOWLEDGEMENT

This research is partially supported by the Intramural Research Program of the National Institutes of Health (NIH), National Library of Medicine (NLM), and Lister Hill National Center for Biomedical Communications (LHNCBC). Mahidol-Oxford Tropical Medicine Research Unit is funded by the Wellcome Trust of Great Britain.

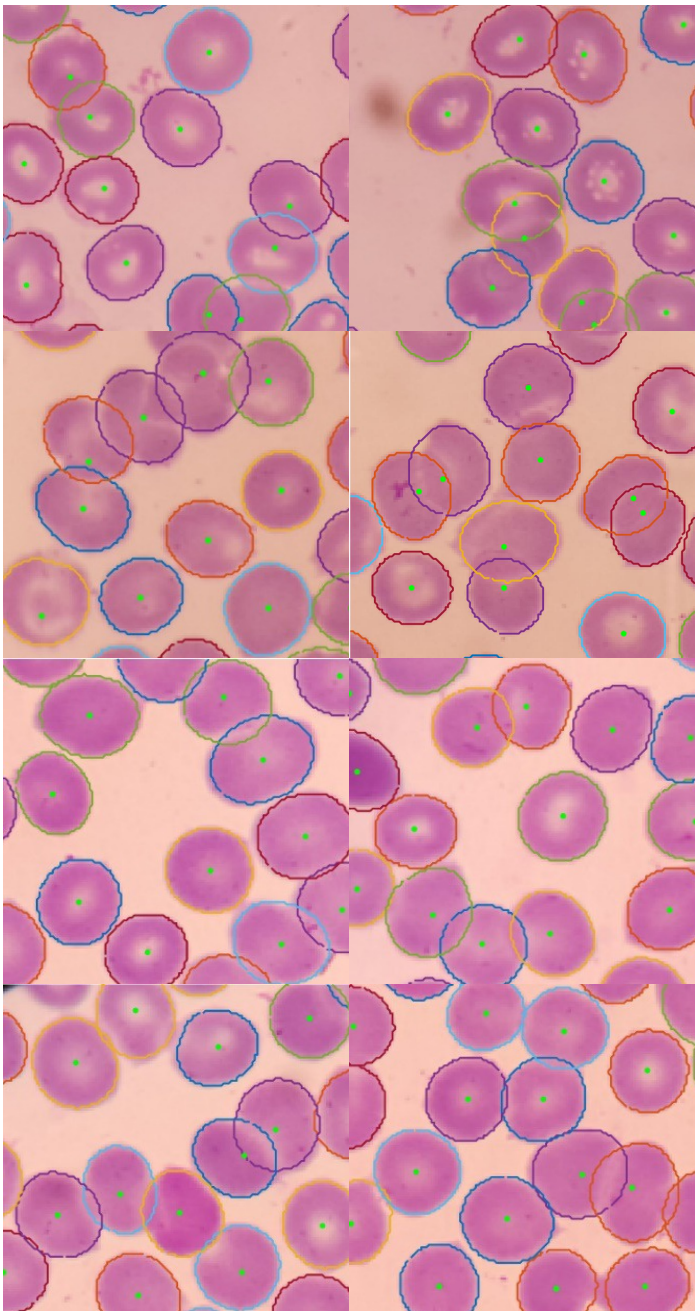

Figure 7. The results for cell detection and cell segmentation demonstrated on sample segments in images from the dataset

REFERENCES

[1] Lichtman, M. A., Beutler, E., Kipps, T. J., Seligsohn, U., Kaushansky, K., and Prchal, J. T., [Williams hematology], McGraw-Hill New York, (2006).

[2] Poostchi, M., Silamut, K., Maude, R., Jaeger, S., Thoma, G., "Image analysis and machine learning for detecting malaria", Translational Research, Available online 12 January 2018, ISSN 1931-5244, https://doi.org/10.1016/j.trsl.2017.12.004, (2018).

[3] Moallem, G., Poostchi, M., Yu, H., Silamut, K., Palaniappan, N., Antani, S., Hossain, M., Maude, R. J., Jaeger, S., Thoma, G. "Detecting and Segmenting White Blood Cells in Microscopy Images of Thin Blood Smears" IEEE Applied Imagery Pattern Recognition Workshop (AIPR), (to appear), (2017).

[4] Makkapati, V. V. and Pathangay, V., "Adaptive color illumination for microscopes," Communications (NCC), 2011 National Conference on, pp. 1-5, (2011).

[5] Savkare, S. and Narote, S., "Automatic detection of malaria parasites for estimating parasitemia," International Journal of Computer Science and Security (IJCSS), vol. 5, p. 310, (2011).

[6] Anggraini, D., Nugroho, A. S., Pratama, C., Rozi, I. E., Pragesjvara, V. and Gunawan, M., "Automated status identification of microscopic images obtained from malaria thin blood smears using Bayes decision: a study case in Plasmodium falciparum," Advanced Computer Science and Information System (ICACSIS), 2011 International Conference on, pp. 347-352, (2011).

[7] Panchbhai, V. V., Damahe, L. B., Nagpure, A. V., and Chopkar, P. N., "RBCs and parasites segmentation from thin smear blood cell images," International Journal of Image, Graphics and Signal Processing, vol. 4, p. 54, (2012).

[8] Ahirwar, N., Pattnaik, S., and Acharya, B., "Advanced image analysis based system for automatic detection and classification of malarial parasite in blood images," International Journal of Information Technology and Knowledge Management, vol. 5, pp. 59-64, (2012).

[9] May, Z., and Aziz, S. S. A. M., "Automated quantification and classification of malaria parasites in thin blood smears," Signal and Image Processing Applications (ICSIPA), 2013 IEEE International Conference on, pp. 369-373, (2013).

[10] Gatc, J., Maspiyanti, F., Sarwinda, D., and Arymurthy, A. M., "Plasmodium parasite detection on red blood cell image for the diagnosis of malaria using double thresholding," Advanced Computer Science and Information Systems (ICACSIS), 2013 International Conference on, pp. 381-385, (2013).

[11] Malihi, L., Ansari-Asl, K., and Behbahani, A., "Malaria parasite detection in giemsa-stained blood cell images," Machine Vision and Image Processing (MVIP), 2013 8th Iranian Conference on, pp. 360-365, (2013).

[12] Das, D., Mukherjee, R., and Chakraborty, C., "Computational microscopic imaging for malaria parasite detection: a systematic review," Journal of microscopy, vol. 260, pp. 1-19, (2015).

[13] Suradkar, P. T., "Detection of malarial parasite in blood using image processing," International Journal of Engineering and Innovative Technology (IJEIT), vol. 2, (2013).

[14] Fang, Y., Xiong, W., Lin, W., and Chen, Z., "Unsupervised malaria parasite detection based on phase spectrum," Engineering in Medicine and Biology Society, EMBC, 2011 Annual International Conference of the IEEE, pp. 7997-8000, (2011).

[15] Purwar, Y., Shah, S. L., Clarke, G., Almugairi, A., and Muehlenbachs, A., "Automated and unsupervised detection of malarial parasites in microscopic images," Malaria Journal, vol. 10, p. 364, (2011).

[16] Bibin, D. and Punitha, P. "Stained blood cell detection and clumped cell segmentation useful for malaria parasite diagnosis," Multimedia Processing, Communication and Computing Applications, ed: Springer, pp. 195-207, (2013).

[17] Khot, S., and Prasad, R., "Optimal computer based analysis for detecting malarial parasites," Proceedings of the 3rd International Conference on Frontiers of Intelligent Computing: Theory and Applications (FICTA) 2014, pp. 69-80, (2015).

[18] Mao-Jun, S., Zhao-bin, W., Hong-Juan, Z.,and Yi-de, M., "A new method for blood cell image segmentation and counting based on PCNN and autowave," Communications, Control and Signal Processing, 2008. ISCCSP 2008. 3rd International Symposium on, pp. 6-9, (2008).

[19] Khan, N. A., Pervaz, H., Latif, A. K., and Musharraf, A., "Unsupervised identification of malaria parasites using computer vision," Computer Science and Software Engineering (JCSSE), 2014 11th International Joint Conference on, pp. 263-267, (2014).
[20] Nasir, A. A., Mashor, M., and Mohamed, Z., "Segmentation based approach for detection of malaria parasites using moving k-means clustering," Biomedical Engineering and Sciences (IECBES), 2012 IEEE EMBS Conference on, pp. 653-658, (2012).
[21] Suryawanshi, M. S., and Dixit, V., "Improved technique for detection of malaria parasites within the blood cell images," Int. J. Scientific & Engg Resrch, vol. 4, (2013).
[22] Wahyuningrum, R. T., and Indrawan, A. K., "A Hybrid Automatic Method For Parasite Detection And Identification Of Plasmodium Falciparum In Thin Blood Images," International Journal of Academic Research, vol. 4, (2012).
[23] Hari, J., Prasad, A. S., and Rao, S. K., "Separation and counting of blood cells using geometrical features and distance transformed watershed," Devices, Circuits and Systems (ICDCS), 2014 2nd International Conference on, pp. 1-5 , (2014).
[24] Khan, M. I., Acharya, B., Singh, B. K., and Soni, J., "Content based image retrieval approaches for detection of malarial parasite in blood images," International Journal of Biometrics and Bioinformatics (IJBB), vol. 5, p. 97, (2011).
[25] Špringl, V., "Automatic malaria diagnosis through microscopy imaging," Faculty Of Electrical Engineering, p. 128, (2009).
[26] Das, D., Ghosh, M., Chakraborty, C., Maiti, A. K., and Pal, M., "Probabilistic prediction of malaria using morphological and textural information," Image Information Processing (ICIIP), 2011 International Conference on, pp. 1-6, (2011).
[27] Ma, C., Harrison, P., Wang, L., and Coppel, R. L., "Automated estimation of parasitaemia of Plasmodium yoelii-infected mice by digital image analysis of Giemsa-stained thin blood smears," Malaria journal, vol. 9, p. 348, (2010).
[28] Zou, L.-h., Chen, J., Zhang, J., and Garcia, N., "Malaria cell counting diagnosis within large field of view," Digital Image Computing: Techniques and Applications (DICTA), 2010 International Conference on, pp. 172-177, (2010).
[29] Maitra, M., Gupta, R. K., and Mukherjee, M., "Detection and counting of red blood cells in blood cell images using Hough transform," International journal of computer applications, vol. 53, (2012).
[30] Venkatalakshmi, B., and Thilagavathi, K., "Automatic red blood cell counting using hough transform," Information & Communication Technologies (ICT), 2013 IEEE Conference on, pp. 267-271, (2013).
[31] Ge, J., Gong, Z., Chen, J., Liu, J., Nguyen, J., Yang, Z., "A system for counting fetal and maternal red blood cells," IEEE Transactions On Biomedical Engineering, vol. 61, pp. 2823-2829, (2014).
[32] Di Ruberto, C., Dempster, A., Khan, S., and Jarra, B., "Analysis of infected blood cell images using morphological operators," Image and vision computing, vol. 20, pp. 133-146, (2002).
[33] Kumarasamy, S. K., Ong, S., and Tan, K. S., "Robust contour reconstruction of red blood cells and parasites in the automated identification of the stages of malarial infection," Machine Vision and Applications, vol. 22, pp. 461-469, (2011).
[34] Sio, S. W., Sun, W., Kumar, S., Bin, W. Z., Tan, S. S., Ong, S. H., "MalariaCount: an image analysis-based program for the accurate determination of parasitemia," Journal of microbiological methods, vol. 68, pp. 11-18, (2007).
[35] Wold, S., Esbensen, K., and Geladi, P., "Principal component analysis," Chemometrics and intelligent laboratory systems, vol. 2, pp. 37-52, (1987).
[36] Jianzhuang, L., Wenqing, L., and Yupeng, T., "Automatic thresholding of gray-level pictures using two-dimension Otsu method," Circuits and Systems, 1991. Conference Proceedings, China., 1991 International Conference on, pp. 325-327, (1991).
[37] https://www.labce.com/spg579129_red_blood_cell_rbc_color_variation.aspx.
[38] Comaniciu, D., and Meer, P., "Mean shift: A robust approach toward feature space analysis," IEEE Transactions on pattern analysis and machine intelligence, vol. 24, pp. 603-619, (2002).

[39] Moallem, G., "Detection and Segmentation of Overlapping Red Blood Cells in Microscopic Medical Images of Stained Peripheral Blood Smears," Master of Sciences, Electrical and Computer Engineering, Texas Tech University, (2017).
[40] Xu, C., and Prince, J. L., "Snakes, shapes, and gradient vector flow," IEEE Transactions on image processing, vol. 7, pp. 359-369, (1998).
[41] Poostchi, M., Ersoy, I., Bansal, A., Palaniappan, K., Antani, S., Jaeger, S., Thoma, G., "Image analysis of blood slides for automatic malaria diagnosis," proceedings of HI-POCT, vol. 15, (2015).
[42] Liang, Z., Powell, A., Ersoy, I., Poostchi, M., Silamut, K., Palaniappan, K., Guo, P., Hossain, M., Antani, S.K., Maude, R.J., Huang, J., Jaeger, S., Thoma, G., "CNN-Based Image Analysis for Malaria Diagnosis" IEEE Int. Conf. on Bioinformatics and Biomedicine (BIBM), pp. 493-496, (2016).
[43] Higgins, J. M., Eddington, D. T., Bhatia, S. N., and Mahadevan, L., "Statistical dynamics of flowing red blood cells by morphological image processing," PLoS computational biology, vol. 5, p. e1000288, (2009).
[44] Ersoy, I., Bunyak, F., Higgins, J. M., Palaniappan, K. "Coupled Edge Profile Active Contours For Red Blood Cell Flow," (2012).